AGU ADVANCING EARTH AND SPACE SCIENCE

Water Resources Research

RESEARCH ARTICLE
10.1029/2020WR027600

Gas Component Transport Across the Soil-Atmosphere Interface for Gases of Different Density: Experiments and Modeling

L. M. Bahlmann[1], K. M. Smits[2,3], K. Heck[4], E. Coltman[4], R. Helmig[4], and I. Neuweiler[1]

[1]Institute of Fluid Mechanics and Environmental Physics in Civil Engineering, Leibniz Universität Hannover, Hanover, Germany, [2]Department of Civil Engineering, University of Texas at Arlington, Arlington, TX, USA, [3]Department of Civil and Environmental Engineering, Colorado School of Mines, Golden, CO, USA, [4]Institute for Modeling Hydraulic and Environmental Systems, Universität Stuttgart, Stuttgart, Germany

Abstract We investigate the influence of near-surface wind conditions on subsurface gas transport and on soil-atmosphere gas exchange for gases of different density. Results of a sand tank experiment are supported by a numerical investigation with a fully coupled porous medium-free flow model, which accounts for wind turbulence. The experiment consists of a two-dimensional bench-scale soil tank containing homogeneous sand and an overlying wind tunnel. A point source was installed at the bottom of the tank. Gas concentrations were measured at multiple horizontal and vertical locations. Tested conditions include four wind velocities (0.2/1.0/2.0/2.7 m/s), three different gases (helium: light, nitrogen: neutral, and carbon dioxide: heavy), and two transport cases (1: steady-state gas supply from the point source; 2: transport under decreasing concentration gradient, subsequent to termination of gas supply). The model was used to assess flow patterns and gas fluxes across the soil surface. Results demonstrate that flow and transport in the vicinity of the surface are strongly coupled to the overlying wind field. An increase in wind velocity accelerates soil-atmosphere gas exchange. This is due to the effect of the wind profile on soil surface concentrations and due to wind-induced advection, which causes subsurface horizontal transport. The presence of gases with pronounced density difference to air adds additional complexity to the transport through the wind-affected soil layers. Wind impact differs between tested gases. Observed transport is multidimensional and shows that heavy as well as light gases cannot be treated as inert tracers, which applies to many gases in environmental studies.

Key Points:
- We assess the effect of near-surface wind on the transport of gas components with different densities in fine sand
- Laboratory experiments are complemented with a fully coupled porous medium-free flow model
- An increase in wind velocity accelerates soil-atmosphere gas exchange. However, the effect differs depending on the gas density

Supporting Information:
- Supporting Information S1

Correspondence to:
L. M. Bahlmann,
bahlmann@hydromech.uni-hannover.de

Citation:
Bahlmann, L. M., Smits, K. M., Heck, K., Coltman, E., Helmig, R., & Neuweiler, I. (2020). Gas component transport across the soil-atmosphere interface for gases of different density: Experiments and modeling. *Water Resources Research*, *56*, e2020WR027600. https://doi.org/10.1029/2020WR027600

Received 1 APR 2020
Accepted 29 JUL 2020
Accepted article online 3 AUG 2020

1. Introduction

Understanding the processes that determine gas exchange at the soil-atmosphere interface is of particular interest in current discussions on climate change. Soil is one of the major sources of greenhouse gas emissions, and atmospheric research and climate modeling rely on precise quantification of emission rates (Oertel et al., 2016). Next to natural production and consumption processes, significant contributions stem from subsurface anthropogenic sources such as landfills (Lou & Nair, 2009) or leaky natural gas infrastructure (Chamindu Deepagoda, Smits, & Oldenburg, 2016; Ulrich et al., 2019). Accurate prediction of soil gas emissions from such sources requires a thorough understanding of the transport mechanisms taking place in the upper vadose zone and at the soil surface as well as suitable models that describe such processes.

Gas movement through soils is caused by concentration gradients (diffusion) and by driving forces such as gradients of temperature (convection), density (buoyancy), and pressure (advection). Resulting transport rates are limited by the properties of the soil (e.g., permeability, porosity, water content) and the properties of the present gases (e.g., gas density, viscosity, diffusivity) (Scanlon et al., 2001). In the vicinity of the soil surface, flow and transport is coupled to the overlying atmosphere by exchange of mass, momentum, and energy. Thus, atmospheric conditions such as barometric pressure, air temperature, and the near-surface wind field define controlling boundary conditions to the transport below. The presence of wind has shown to be a relevant factor in influencing subsurface gas transport and exchange rates between soil and atmosphere. Wind is commonly understood to increase soil gas emissions (e.g., Levintal et al., 2019; Maier et al., 2012; Poulsen & Sharma, 2011) and evaporation rates (Acharya & Prihar, 1969; Davarzani et al., 2014; Fetzer et al., 2016; Hanks & Woodruff, 1958; Ishihara et al., 1992). This is supported by observations made in the

field and under natural conditions (e.g., Bowling & Massman, 2011; Laemmel et al., 2017; Levintal et al., 2019; Massman et al., 1997; Maier et al., 2010; Mohr et al., 2016; Poulsen & Møldrup, 2006). Since the underlying mechanisms to the effect are still largely unidentified, a considerable effort has been put into investigating wind effects on soil gas transport under controlled laboratory conditions (Chamindu Deepagoda, Smits, & Oldenburg, 2016; Maier et al., 2012; Pourbakhtiar et al., 2017; Poulsen, Pourber, et al., 2017). In general, these studies show that the extent of wind impact increases with wind speed. The experimental design in such studies is often based on the assumption that the transport in a porous medium with an overlying wind field is one-dimensional occurring primarily in vertical direction. The main mechanism behind the wind impact is assumed to be *turbulence-induced pressure pumping*. With increasing wind speed a wind field becomes turbulent. The high-frequency oscillations of pressure in a turbulent near-surface wind field are expected to transfer into the soil and cause fast changing, multidirectional advection. Although net advective transport is assumed to be zero, fluctuations cause enhanced dispersive mixing in addition to molecular diffusion (Levintal et al., 2019). As turbulence increases for higher wind speeds, dispersion also increases, hence, the correlation between wind speed and the extent of wind impact on subsurface gas transport.

More recent studies suggest that the abovementioned assumptions about the underlying mechanisms of wind impact on subsurface gas movement have to be taken under consideration. In several consecutive studies Poulsen, Furman, and Liberzon (2017, 2018) and Poulsen (2018, 2019) showed that near-surface winds can cause both vertical and horizontal gas transport, suggesting the presence of wind-induced horizontal advection. This was shown for highly permeable materials (gravel, crushed granite, and coarse sand with air permeability $>1e-9\ m^2$). Poulsen et al. (2018) investigated gas transport from an initially saturated soil tank under different wind speeds and different modes of wind gustiness. Concentration values were observed at different horizontal and vertical locations inside the tank. Results indicate that transport inside the porous medium becomes increasingly multidimensional with increasing near-surface wind speed. In Poulsen (2018, 2019) experiments were set up to directly visualize wind-induced horizontal advection at different depths. It was shown that horizontal pore velocity increases with wind speed and wind gustiness. The effect decreases with porous medium depth, which is likely due to dissipation of the momentum transferred at the surface by friction. It is unclear how much this mechanism contributes to soil-atmosphere gas exchange in comparison to turbulence-induced pressure pumping. If wind-induced horizontal gas transport shows to be a relevant factor, this not only has significant implications for calculating or describing soil gas emission rates but also for other fields of interest such as the spreading of gaseous contaminants in the vadose zone. Further investigation on its occurrence should be considered. Especially since its limitations are not yet investigated. Although results in Poulsen (2019) suggest that horizontal gas transport reduces with a decrease in air permeability of the porous medium, it is unclear if wind-induced horizontal gas movement is relevant in less permeable materials such as fine sands and nongranular soils.

Moreover, the gases used in the abovementioned studies are treated as inert tracers. However, these gases as well as most gases of interest in environmental studies are not. For instance, greenhouse gases such as methane CH_4, carbon dioxide CO_2, and nitrous oxide N_2O all show pronounced density differences to air. As such, when soil gases with a different density to air mix with the atmosphere, the resulting density gradients likely influence transport in the vicinity of the soil surface, adding complexity to the transport problem. Although gas density is commonly recognized as a relevant factor on gas transport through soils (Altevogt et al., 2003; Falta et al., 1989; Jang & Aral, 2007), to the author's knowledge, there are no studies available that provide inside on how density gradients affect gas transport close to a wind-exposed soil surface.

In the attempt to determine the driving mechanisms for the transport and exchange of gas components at the interface between the soil and the atmosphere, we are limited by the fact that these mechanisms cannot be measured directly. This is especially problematic, since transport is likely to be caused by several superimposed mechanisms. To overcome this problem, experiments can be supported by numerical investigations. Capturing the processes at the soil-atmosphere interface requires model concepts that couple the porous medium to the overlying free flow region. This can be done by different approaches, which are generally grouped into two categories: one- and two-domain approaches. One-domain models solve a single set of transport equations for both the porous medium and the free flow (e.g., Basirat et al., 2015). In two-domain models the porous medium and the free flow regions are separated by a sharp interface. Each

domain is solved by an individual set of equations. Coupling conditions at the domain intersection account for the exchange of mass, momentum, and energy. Such concepts provide the possibility of detailed modeling of the free flow while still applying simplifying assumptions to the porous medium (Fetzer et al., 2016). In recent years, such models have been increasingly applied to analyze effects of wind on evaporation from bare soils (e.g., Fetzer et al., 2016; Gao et al., 2018; Haghighi & Or, 2015). To the authors' knowledge, such models have yet to be used to investigate wind effects on pure soil gas transport problems, especially, to unravel the contribution of competing mechanisms. Although Basirat et al. (2015) investigated transport of carbon dioxide through a coupled domain of porous medium and free air space by designing an experiment and applying a one-domain model, the influence of wind was not included into the investigation, as no wind field was applied to the free air space. Adding such coupled models to the experimental investigation of wind effects on subsurface transport could be the crucial step toward determining the underlying mechanisms to observed transport phenomena.

The main objective of this study is to deepen the understanding of gas transport mechanisms in the near-surface soil layers and at the interface between soil and atmosphere under the presence of near-surface winds. For the first time, we provide a study that considers density effects on the transport: Wind influence on subsurface gas transport is tested comparatively for gases with varying density. We follow an approach combining laboratory experiments with a fully coupled porous medium-free flow model considering turbulent flow in the atmosphere to be able to capture the relevant transport mechanisms. Laboratory experiments were performed at bench scale in a quasi two-dimensional sand tank with an overlying wind tunnel. Tested conditions include four different wind velocities and three gases, a light, a heavy, and a quasi density-neutral gas. The possibility of wind causing multidimensional transport phenomena was taken into account by measuring soil gas concentrations at multiple horizontal and vertical locations inside the tank. Concentrations were measured continuously for two distinctly different cases of gas transport: steady-state gas supply from a buried point source and subsequent transient transport from the partially saturated sand tank, which is initiated by stopping the gas supply. We consider that wind influence differs between those two cases. Concentration measurements were collected to test theory and to validate the numerical model for both modes of transport. The model was fitted and subsequently used to identify the main transport mechanisms at the interface.

2. Experimental Design

An experimental design was developed that allows to test quasi two-dimensional gas transport through soils under varying wind conditions. The setup is adaptable for different gases. It was inspired by previous gas transport and evaporation experiments in coupled systems of porous medium and free flow, where a sand tank is placed underneath a wind tunnel (Chamindu Deepagoda et al., 2018; Chamindu Deepagoda, Smits, & Oldenburg, 2016; Davarzani et al., 2014). Such systems allow for high control over test conditions and possess clearly defined domain boundaries for both the porous medium and the overlying wind field, which is ideal for subsequent numerical studies.

2.1. Experimental Setup

The setup consists of a $55 \times 36 \times 8$ cm ($l \times h \times w$) sand tank and an open return wind tunnel with an overall length of 4.4 m and a rectangular cross section of 25×8 cm (see Figure 1). Downstream of the interface between wind tunnel and sand tank, the wind tunnel transforms into a circular duct, which holds an in-line duct fan (Suncourt Pro Model DB6GTP, 15.2 cm). The fan generates airflow by suction. It is regulated by a variable velocity controller and a galvanized circular damper as has been done by Chamindu Deepagoda, Smits, and Oldenburg (2016). A thermal anemometer (TSI, Alnor velometer AVM440, range 0–30 m/s, accuracy 3% of reading or 0.015 m/s) is placed inside the tunnel above the soil tanks vertical center line to scan the wind velocity profile. It additionally measures air temperature (accuracy 0.3°C) and relative humidity (accuracy 3%). Additional temperature and humidity sensors (Decagon Devices, Inc. EHT RH/Temperature, RH accuracy $\pm$2% and temperature accuracy $\pm$0.25°C) are installed upstream and downstream of the interface. All sensor data are collected using a CR1000 Campbell Scientific data logger.

An integrated sensor network is embedded into the sand tank for high-resolution measurements of gas component concentration, soil temperature, and soil moisture distributions. The sensors are integrated into the tank walls. Refer to supporting information Figure S1 for exact sensor placements. The back of the tank is

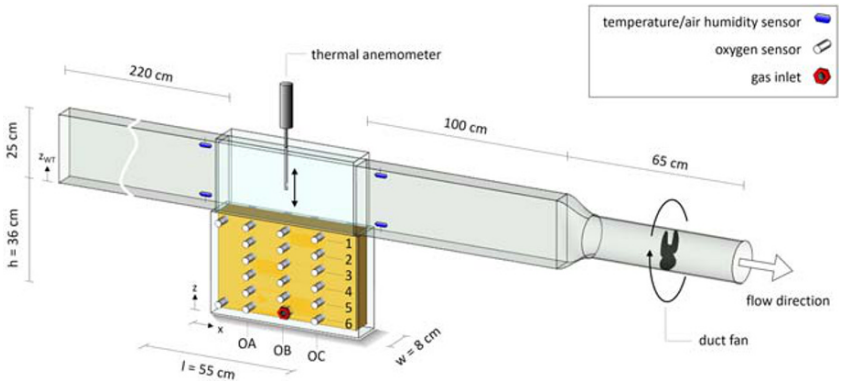

Figure 1. Schematic diagram of the porous medium-wind tunnel experiment.

equipped with two vertical lines of temperature sensors (ST-100 Thermistor Sensors, Apogee Instruments, self-calibrating, accuracy 0.1°C) and four lines of soil moisture sensors, which were installed for subsequent experiments on gas component transport in partially saturated soil, which will not be discussed here. The front of the tank is equipped with 17 oxygen sensors (Figaro KE25, range 0–100%, accuracy 1%), arranged along three vertical transects (OA, OB, and OC; see Figure 1). Two additional sensors are placed at the lower left and upper left corner. Oxygen concentration is measured as percent oxygen c_{O_2} (Vol-%). Since atmospheric oxygen levels inside the laboratory are stable, the oxygen concentration is proportional to the concentration of pure air c_{air}. When the volume of air inside the porous medium reduces due to the replacement by another gas component, the oxygen sensors react inversely proportional, which leads to the following relation between the concentration of the additional component and the oxygen concentration c_{O_2}:

$$c = 100\% - c_{air} = 100\% - \frac{100\%}{21\%} \cdot c_{O_2} \tag{1}$$

Invoking the relation above, the sensors can be used to trace a variety of gases. The same method has been applied by Pourbakhtiar et al. (2017), Poulsen et al. (2018), and Poulsen (2018, 2019) to trace carbon dioxide.

The gas inlet is placed directly above the bottom center of the soil tank, in line with Sensor Row 6. It is constructed out of a cylindrical micron filter element that reaches across the width of the tank to achieve a relatively uniform injection across the tank width to limit the possibility of 3-D effects. Thus, in two dimensions, the gas inlet can be represented as a point source. The inlet connects to a pressurized gas cylinder. Gas supply is controlled by a regulation valve and a mass flow meter (Omega, model FMA-1607A, range 0.05 to 10 slpm, accuracy 0.8%). An inflow rate of 0.5 slpm (= 0.2 mol/s) was applied, representing a diffusion-dominant leak from a shallow subsurface source, as described in Chamindu Deepagoda, Smits, and Oldenburg (2016) and also in Ulrich et al. (2019). Chamindu Deepagoda, Smits, and Oldenburg (2016) found measurable influences of wind velocity on the concentration profile inside the soil and on concentrations above the soil surface. As tested wind conditions and setup dimensions are in accordance with our study, we chose to use the same flow rate.

2.2. Soil Characteristics

The tank was filled with uniform specialty silica sand, Accusand 50/70 (identified by the effective sieve number). Accusand 50/70 is a laboratory-grade quartz sand (99.8% quartz) with a grain shape classified as rounded. It has been widely used in experimental investigations of transport processes in porous media, and its hydraulic and thermal properties have been thoroughly investigated. Relevant properties can be found in Chamindu Deepagoda, Smits, Ramirez, and Moldrup (2016) and Smits et al. (2010). The sand was oven dried prior to packing. Maximum packing densities were established by packing in 5 cm increments and applying standard compacting methods in order to maximize homogeneity. The characteristics of the sand are listed in Table 1.

Table 1
Properties of Uniform Specialty Silica Sand, Accusand 50/70 Under Tight Packing Conditions

Mean particle diameter (mm)[a]	Particle density (g/cm^3)[b]	Particle sphericity (—)[b]	Bulk density (g/cm^3)[b]	Porosity ϕ (cm^3/cm^3)	Air permeability k (m^2)[b]
0.26	2.659	0.909	1.77	0.33	1e − 11

[a]Glass et al. (2000). [b]Chamindu Deepagoda, Smits, Ramirez, and Moldrup (2016).

2.3. Tested Conditions

Experiments were conducted using three different gases: carbon dioxide CO_2, nitrogen N_2, and helium He. Each of the gases was tested under four different wind conditions, resulting into a total of 12 experiments. Gas properties are listed in Table 2. The gases were chosen, because they are nonreactive, nontoxic, and nonexplosive, and they significantly differ in molecular weight, which directly influences their density ρ and their molecular diffusion coefficient D_m. CO_2 is approximately 1.5 times heavier than pure air, N_2 serves as a density-neutral gas, and He is comparably light (7 times lighter than air). The diffusion coefficients decrease with increasing molecular weight. Differences in dynamic viscosity are less pronounced.

The four tested Wind Conditions W1, W2, W3, and W4 are distinguished by their time averages of wind velocity measured at the wind tunnel center point $\overline{v}(z_{wt} = 12.5\,\text{cm}$. W1 leads to mean velocities of approximately 0.2 m/s. W2, W3, and W4 correspond to 1.0, 2.0, and 2.7 m/s, respectively. Examples of measurements are given in Figure 2. Figure 2a shows measurements of $v(z_{wt} = 12.5\,\text{cm})$. Variation around the time average increases with increasing wind velocity. More specifically, we observe an increase in amplitude and frequency.

All conducted experiments are listed in Table 3. For selected experimental conditions, replicate experiments were carried out to confirm conditions and repeatability. Atmospheric temperatures inside the laboratory, T, remained constant throughout all experiments, whereas local changes in weather caused variations in relative humidity, RH, from 33% to 63%. As can be seen by listed measurements of $\overline{v}(z_{wt} = 12.5\,\text{cm}$, the replication of Wind Conditions W1, W2, W3, and W4 was successful. The desired time-averaged velocity of each wind condition is met with maximum deviations of 0.04 m/s.

2.4. Experimental Procedure

Each of the 12 experiments followed the two-step procedure illustrated in Figure 3. First, wind conditions were established, and the wind velocity profile inside the wind tunnel was scanned by adjusting the height of the anemometer and measuring the velocity at 1, 2.5, 5, 7.5, 10, 12.5, 15, 17.5, 20, and 22.5 cm above the soil surface with a frequency of one measurement per second for 100 s. Subsequently, gas supply was turned on, and the inflow rate was set to 0.5 slpm until a steady-state concentration distribution was established (Transport Case 1). To confirm that steady-state conditions were achieved, oxygen concentrations were continuously monitored at all sensor locations until time-invariant concentrations were recorded for at least 15 min. Subsequently, a second transport case was initiated by stopping the gas supply. The duct fan remained turned on, and data collection continued until the oxygen sensors indicated all gas (He, CO_2, or N_2) had left the tank. This two-step procedure allows us to observe two distinctly different cases of component transport. Case 1: During the steady-state case, transport through the coupled system is strongly

Table 2
Gas Component Properties at Normal Atmospheric Conditions ($T = 20°C$ and $p = 101.325\,kPa$)

Gas	Symbol	Molar mass M (g/mol)	Density ρ (kg/m^3)	Dynamic viscosity μ(Pa·s)[a]	Molecular diffusion coefficient D_m (cm^2/s)[b]
Pure air	air	29	1.21	1.83e − 5	0.189
Carbon dioxide	CO_2	44.01	1.84	1.47e − 5	0.155
Nitrogen	N_2	28.02	1.17	1.76e − 5	0.195
Helium	He	4.02	0.17	1.96e − 5	0.669

[a]Reid et al. (1959). [b]Binary diffusion coefficient for a gas diffusing through air (Fuller method, Equation 4).

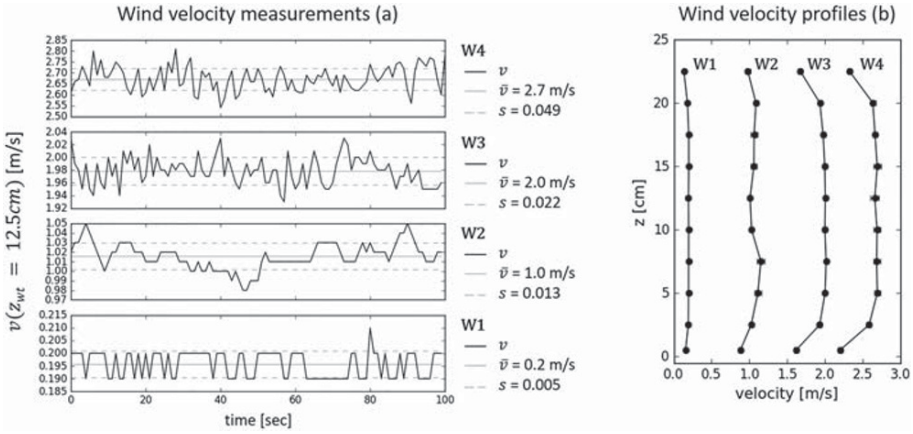

Figure 2. Wind velocity measurements. (a) Exemplary measurements taken at the wind tunnel center point. Solidgray lines show the time averages v, and gray dashed lines show standard deviations s. (b) Exemplary profiles oftime-averaged velocity measurements.

influenced by the advective flux applied at the gas inlet. Case 2: Once the gas is stopped, diffusion is likely to be the main contributor to the transport of the gas molecules. It is to be expected that wind effects differ between those two cases. Throughout the procedure, oxygen concentrations and soil temperatures were monitored every 5 s. Conditions in the wind tunnel (air temperature and RH) were scanned once every minute.

3. Model Concept

The sand and the overlying wind field are simulated as a coupled system of a porous medium and a free flow domain (two-domain approach). The domains are separated by a sharp interface. Flow and transport through the domains are modeled by two different sets of equations. The domains are connected via coupling conditions to account for mass and momentum exchange. Flow in the porous medium is described through Darcy's law, where flow follows pressure gradients. For the wind tunnel, we solve Reynolds-averaged Navier-Stokes (RANS) equations. In both domains we solve isothermal transport of two components through a single gaseous phase (the main component *air* and the injected component He, N_2, or CO_2). Temperature differences are neglected since experimental results showed no noticeable temperature gradients within the soil or between the soil and the surrounding atmosphere.

All equations are discretized using a cell-centered finite volume method in the porous medium and a staggered grid method in the free flow. The system is solved fully implicitly. The model is implemented in the numerical software framework DuMu^x (Koch et al., 2020) where more information on the implementation of the coupling concept and on the discretization methods can be found. In the following, we present the basic equations behind the model.

3.1. Flow and Transport Inside the Porous Medium

The transport of a component i in the gas phase of a porous medium with porosity ϕ can generally be described by a mass balance equation including advection and diffusion as transport mechanisms

$$\frac{\partial\left(\phi\varrho X^i\right)}{\partial t} + \nabla\left(j^i_{\mathrm{A}} + j^i_{\mathrm{D}}\right) = q^i \text{ with } j^i_{\mathrm{A}} = \varrho X^i \boldsymbol{v} \text{ and } j^i_{\mathrm{D}} = -\varrho D_{\mathrm{eff}} \nabla X^i \tag{2}$$

where X^i (kg/kg) is the component mass fraction, ϱ (kg/m^3) is the density of the gas mixture, and q^i (kg/m^3/s) represents sources and sinks. Diffusive transport j_{D} is described by Fick's law, which is valid in a binary system when Knudsen effects do not play a role. Knudsen effects become relevant for low permeable soils such as clay. It was shown that Fick's law performs well for transport through higher permeable materials such as the fine sand used in the present study (Bear, 1961; Sleep, 1998). The law depends on the concentration gradient and the effective diffusion coefficient D_{eff} (m^2/s), which is calculated from

Table 3
Experiments and Respective Measurements of Atmospheric Conditions: Time-Averaged Wind Velocity $\overline{v}(z_{wt} = 12.5\text{cm}$, *Air Temperature* $\overline{T}$, *and Relative Humidity* $\overline{RH}$

Experiment ID	Gas type	Wind condition	$\overline{v}$ (m/s)	T (°C)	RH (%)
CO_2-W1	CO_2	W1 ≈ 0.2 m/s	0.22	20.4	61
CO_2-W2		W2 ≈ 1.0 m/s	1.02	20.2	45
CO_2-W3		W3 ≈ 2.0 m/s	2.03	19.9	61
CO_2-W4		W4 ≈ 2.7 m/s	2.71	20.1	57
He-W1	He	W1 ≈ 0.2 m/s	0.20	20.4	61
He-W2		W2 ≈ 1.0 m/s	0.99	20.2	60
He-W3		W3 ≈ 2.0 m/s	2.00	20.4	58
He-W4		W4 ≈ 2.7 m/s	2.69	20.2	49
N_2-W1	N_2	W1 ≈ 0.2 m/s	0.22	20.5	53
N_2-W2		W2 ≈ 1.0 m/s	1.03	19.9	45
N_2-W3		W3 ≈ 2.0 m/s	2.04	20.3	63
N_2-W4		W4 ≈ 2.7 m/s	2.74	19.8	58

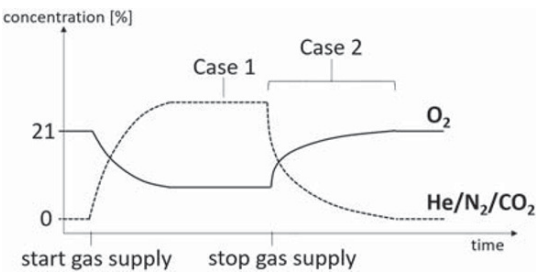

Figure 3. The experimental procedure: With the start of constant gas supply, oxygen concentrations inside the sand tank are monitored in real time until a steady-state concentration distribution establishes (Case 1). Subsequently, gas supply is stopped to introduce transient transport under decreasing concentration gradients (Case 2).

molecular diffusion D_m (m^2/s). We account for tortuosity by factoring D_m with the coefficient τ (—) and for dispersion by including a velocity-dependent dispersion term with scaling parameter α (m) (Scheidegger, 1961):

$$D_{eff} = \phi \cdot \tau \cdot D_m + \alpha v \tag{3}$$

Molecular diffusion coefficients D_m of a binary gas mixture consisting of components i and j are calculated using the Fuller method (Reid et al., 1959)

$$D_m = \frac{0.00143T^{1.75}}{pM_{ij}^{1/2}\left(V_{at,i}^{1/3} + V_{at,j}^{1/3}\right)^2} \tag{4}$$

with V_{at} (—) as the atomic diffusion volumes of each component and M_{ij} (g/mol) as the average molar mass of the mixture. The coefficient varies with temperature T (K) and pressure p (Pa). Advective transport j_A is determined by the flow field. The velocity vector $\boldsymbol{v}$ (m/s) is described by Darcy's law. Thereby, flow is driven by gradients of pressure p and gravity $\mathbf{g}$ and is limited by the intrinsic permeability of the porous medium k (m^2) and the dynamic viscosity of the gas phase μ (Pa·s):

$$\boldsymbol{v} = \frac{k}{\mu}(\nabla p - \varrho \mathbf{g}) \tag{5}$$

In the presence of advection, gas-phase density and viscosity become relevant factors to the transport. These fluid state variables are highly dependent on the composition of the gas mixture. The density is calculated from ideal gas law and Dalton's law as

$$\varrho = \frac{p}{RT}\sum_i M_i x_i \tag{6}$$

with M_i as the molar mass of a component i and x_i as the respective molar fraction (Helmig, 1997). R represents the universal gas constant. The dynamic viscosity is calculated applying the Wilke method (Reid et al., 1959). Thereby μ relates to the composition of the gas phase with

$$\mu = \sum_i \frac{x_i \mu_i}{\sum_j x_j \phi_{ij}} \tag{7}$$

where μ_i is the viscosity of the pure component i and ϕ_{ij} is defined as

$$\phi_{ij} = \frac{(1 + (\mu_i/\mu_j)^{1/2}(M_j/M_i)^{1/4})^2}{(8(1 + M_i/M_j))^{1/2}} \tag{8}$$

3.2. Flow and Transport Inside the Free Flow Domain

With increasing flow velocities a wind field potentially becomes turbulent. To predict the characteristics of such flow fields, suitable mathematical models must be applied. Turbulent flows are usually simulated by solving the Navier-Stokes equations. Since the direct solution of these equations is computational expensive, the equations are simplified by Reynolds decomposition. Thereby, the pressure and the velocity of the fluid flow are decomposed into their time averages and a fluctuating part, which gives the RANS equations. For derivation of the RANS equations

we refer to classical fluid dynamics text books such as Wilcox (1993). Reynolds averaging leads to the following description of mass and momentum balance for a component i:

$$\frac{\partial \varrho \overline{X}^i}{\partial t} + \nabla \cdot \varrho \overline{\boldsymbol{v}} \overline{X}^i - (D_\mathrm{m} + D_\mathrm{t}) \varrho \nabla \overline{X}^i - q^i = 0 \tag{9}$$

$$\frac{\partial (\varrho \overline{\boldsymbol{v}})}{\partial t} + \nabla \cdot \left(\varrho \overline{\boldsymbol{v}} \overline{\boldsymbol{v}}^T \right) = \nabla \cdot \left((\varrho \nu + \varrho \nu_\mathrm{t}) \left(\nabla \overline{\boldsymbol{v}} + \nabla \overline{\boldsymbol{v}}^T \right) \right) - \nabla \overline{p} + \varrho \mathbf{g} \tag{10}$$

Time-averaged quantities are denoted by bars (e.g., $\overline{v}$). Additional quantities resulting from the averaging process are the eddy viscosity ν_t (m^2/s) and the eddy diffusivity D_t (m^2/s), which accounts for mixing due to turbulence. Both quantities need approximation by suitable models. D_{tt} can be related to ν_t by the turbulent Schmidt number Sc_t (assume $Sc_t = 1$):

$$D_\mathrm{t} = \frac{\nu_\mathrm{t}}{Sc_\mathrm{t}} \tag{11}$$

The eddy viscosity ν_t acts as a proportionality coefficient in relating the turbulent stresses to the velocity gradient. To compute ν_{tt}, several models are available. In the present study, the algebraic turbulence model by van Driest is applied (Van Driest, 1956). The model is based on Prandlt's mixing length theory that proposes, ν_t can be approximated as the product of velocity gradient and a characteristic mixing length l:

$$\nu_\mathrm{t} = l^2 \left| \frac{\partial u}{\partial y} \right| \tag{12}$$

Suitable representation of the mixing length must be found depending on the flow region. Van Driest's formulation of the mixing length provides a continuous velocity and shear stress distribution for wall-bounded turbulent flows. Thereby l relates to the wall distance y by

$$l = \kappa y (1 - e^{-y^+/26}) \tag{13}$$

where κ is an empirical constant known as the von Kármán's constant and y^+ the wall distance measured in viscous length (related to wall distance y and friction velocity u_τ by$y^+ = y u_\tau / \nu$). Refer to Wilcox (1993) for more detailed information.

3.3. Coupling Conditions

The present model includes a coupling concept that was presented by Mosthaf et al. (2014) and Fetzer et al. (2016). It is based on the assumption of local thermodynamic equilibrium at the interface. As a results, mass exchange is discribes by the continuity of component mass fluxes between the free flow (ff) and the porous medium (pm), here for component κ

$$\left[\varrho \overline{X}^\kappa \overline{\boldsymbol{v}} + j^\kappa_{\mathrm{D,\,ff}} \cdot \mathbf{n} \right]^{\mathrm{ff}} = - \left[\varrho X^\kappa \boldsymbol{v} + j^\kappa_{\mathrm{D,\,pm}} \cdot \mathbf{n} \right]^{\mathrm{pm}} \tag{14}$$

with $\mathbf{n}$ as the interface normal vector (pointing out of the respective domain) and the diffusive fluxes $j_{\mathrm{D,\,ff}}$ and $j_{\mathrm{D,\,pm}}$. The momentum exchange is coupled in both tangential and normal directions. For the tangential momentum, the coupling condition is set according to the Beavers-Joseph-Saffman condition (Beavers & Joseph, 1967; Saffman, 1971):

$$\left[\overline{\boldsymbol{v}} - \frac{\sqrt{(\boldsymbol{k} \boldsymbol{t}_i) \cdot \boldsymbol{t}_i}}{\alpha_\mathrm{BJ} \varrho \nu} \tau_\mathrm{t} \mathbf{n} \cdot \boldsymbol{t}_i \right]^{\mathrm{ff}} = 0 \tag{15}$$

The condition is designed for naturally permeable walls such as the surface of a porous medium. It allows nonzero tangential velocities directly at the interface by replacing the no-slip boundary condition with a slip boundary condition. The properties of the porous medium are accounted for by the dependency on the intrinsic permeability tensor $\boldsymbol{k}$ and a dimensionless material parameter α_BJ. $\boldsymbol{t}_i$ denotes the i th

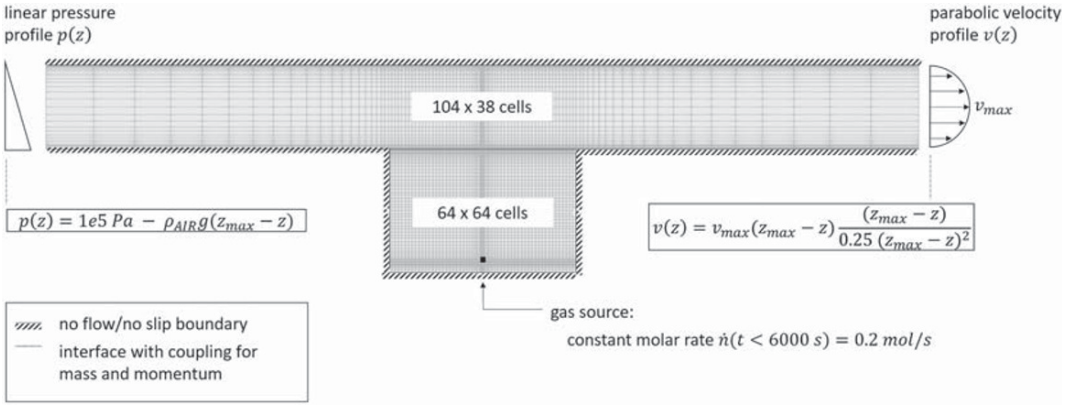

Figure 4. Model geometry and boundary conditions.

linear ndependent interfiace tangential vector, and $\boldsymbol{\tau}_i$ is the turbulent shear stress tensor defined as $\tau_t = (\varrho\nu + \varrho\nu_t)(\Delta\overline{\mathbf{v}} + \Delta\overline{\mathbf{v}}^T)$. For the normal part of the momentum balance, the coupling condition is as follows

$$\left[\left(\left(\varrho, \overline{\mathbf{v}}\overline{\mathbf{v}}^T - \tau_t\ ,+\ ,\overline{p}, \mathbf{I}\right)\mathbf{n}\right) \cdot \mathbf{n}\right]^{\mathrm{ff}} = [p]^{\mathrm{pm}} \tag{16}$$

with $\mathbf{I}$ as the identity matrix.

3.4. Model Setup and Boundary Conditions

Due to the choice of experimental setup, transport inside the porous medium is fully mixed across the sand tank width, which permits a reduction to two dimensions. The reduction is necessary in order to keep affordable computation times. The model consists of a free flow domain of size 100×25 cm interfaced with a porous medium domain of size 55×36 cm (see Figure 4). At the interface, coupling conditions are set for momentum and mass. All walls are set to be no-flow boundaries for pressure and mole fractions. The walls of the free flow additionally contain no-slip boundaries for the velocity. The flow field is driven by the inflow and the outflow boundary of the free flow. We assume that the gas at the inflow (left side) consists entirely of the *air* component. Therefore $x_{He/CO_2/N_2}$ is set to zero, and we assume a hydrostatic pressure profile. At the outflow boundary (right side), we apply a parabolic velocity profile $v_x(z)$, which depends on the maximum flow velocity at the center of the free flow $v_{max}(z = 12.5\ \mathrm{cm})$. The gas inlet is represented by a Neumann boundary condition at the corresponding location. Initial conditions are set for all primary variables (pressure $p = 1e5aPa$, velocity $\overrightarrow{v} = \overrightarrow{0}$ m/s, and mole fraction $x_{He/CO_2/N_2} = 0$). The simulation process follows the experimental procedure (see Figure 2). From the beginning of the simulation, the gas source generates a constant mole rate of 2.5 mol/(m s) (applied molar flux at the inlet divided by the tank width) until a point in time when the flow field and the concentration field in the system are equilibrated. A period of 6,000 s was found to be sufficient. At $t = 6{,}000$ s, the mole rate is set to 0, and the simulation continues for another 14,000 s. A convergence study was carried out for both time and space discretization. All solutions are converging for a grid of 8,048 cells (see Figure 4). The grid is refined around locations of high gradients: around the gas source, at the interface, and toward the walls of the free flow. To resolve the laminar boundary layer, y^+ values are kept lower than 5 for the first three cells closest to the walls. The local grid refinements cause elongated grid cells with relatively high aspect ratios at the interface and the boundaries of the free flow. However, these cell elongations do not affect the numerical solution, which was tested by stepwise reduction of aspect ratios.

4. Experimental Results

The gas concentration distribution under steady-state gas supply (Case 1) and sensor breakthrough curves for the subsequent transient transport (Case 2) are analyzed regarding their sensitivity to gas type and

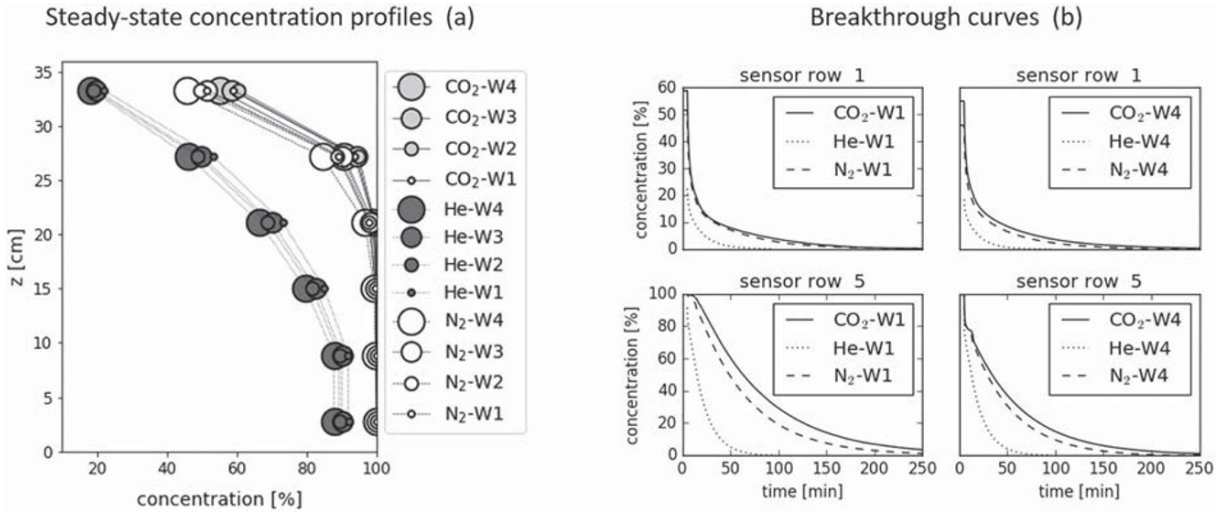

Figure 5. (a) Gas concentration profiles during steady-state gas supply (Transport Case 1). Shown values are horizontally averaged between transects OA, OB, and OC. Marker size increases for increasing wind velocities. (b) Average breakthrough curves for Sensor Rows 1 and 5 for Wind Conditions W1 and W4 (Transport Case 2).

imposed wind condition. We investigate if there is a difference in wind influence between gas types and if we find evidence of wind-induced subsurface advection and turbulence-induced pressure pumping.

4.1. Influence of Gas Type

In general, there are higher differences observed between experiments with different gases than between experiments under different wind conditions. This is valid for both transport cases (see Figure 5). Under steady-state gas supply (Case 1), gas concentrations inside the sand tank increase toward the soil tank bottom. Figure 5a shows the concentration profiles over soil tank depth averaged between transects OA, OB, and OC. For separate profiles we refer to Figure S2. The profiles vary depending on the gas type.

Whereas CO_2 and N_2 fill the entire lower half of the sand tank, He only partly displaces the air out of the pores, likely due to its high diffusion coefficient. As the system is in steady-state, total fluxes out of the soil tank equal the flux applied at the gas inlet. The flux is composed of a diffusive and an advective part, and the ratio between both varies dependent on the location inside the sand tank. Whereas advective flux decreases with distance to the gas inlet, diffusive flux increases toward the soil surface where concentration gradients are strongest. Due to the differences in diffusion coefficients, partitioning into advective and diffusive ratios differs between gases. The lighter the gas, the higher the diffusive ratio. It is likely due to high advective ratios at the bottom that N_2 and CO_2 fill the entire lower half of the tank. Density gradients are expected to increase the difference between the gas distributions. In case of low-density gases such as He, density gradients support upward-directed transport, whereas for heavy gases, density gradients counteract the upward-directed transport.

When gas supply is terminated (start of Case 2), transport is no longer driven by the advective flux enforced by the gas source. Instead, concentration gradients between soil tank and wind tunnel dominate the transport. The wind transports the emerging gas away from the surface, causing low soil surface concentrations. Due to the difference in diffusion coefficients and density gradients, exchange rates between soil and wind tunnel are expected to be noticeably higher for He than for N_2 and CO_2. This is reflected by the measurements, as can be seen in Figure 5b, which displays exemplary breakthrough curves for Wind Conditions W1 and W4. Note that initial conditions for transient transport differ for experiments with different gas types and also to a small extent for experiments under different wind conditions. To investigate the relevance of additional transport mechanisms to the molecular diffusion, we compare transport times observed during the experiments to those of a purely diffusive process. Transport times are derived from sensor breakthrough curves and are generally defined as the time it takes for a sensor concentration to drop from an initial level to a certain new level (e.g., Pourbakhtiar et al., 2017). As comparison criterion between experiments, we use the

Table 4
Comparison of Ratios Between Maximum Measured Transport Times and the Inverse of Corresponding Diffusion Coefficients Dependent on the Imposed Wind Condition

Gas 1	Gas 2	D_1/D_2	$t_{max,2}/t_{max,1}$ W1	W2	W3	W4
He	N_2	**3.43**	3.41	3.43	3.21	2.92
CO_2	N_2	**0.79**	0.75	0.74	0.79	0.77

Note. Values in boldface are the values to which the values in the following columns should be compared.

maximum transport time t_{max}, which is the longest transport time observed in the system and corresponds to sensor OC6. For comparability between gas types, t_{max} is defined as the time it takes for the $He/N_2/CO_2$-concentration to reduce from 88 to 3 Vol-%, which denotes the highest common concentration span at sensor OC6 between all experiments ($t_{max} = \Delta t$ between $c_{OC6} = 88\%$ and $c_{OC6} = 3\%$). The transport time of a purely diffusive process (t_D) is inversely proportional to the diffusion coefficient D (e.g., $t_D = \frac{x^2}{2D}$). Consequently, the ratio of diffusion times between two gases is inverse to the ratio of their diffusion coefficients. This is matched relatively well by ratios of measured transport times as shown in Table 4.

This confirms that molecular diffusion is likely to be the main contributor to transport inside the sand tank during transient transport. However, deviations between the ratios also indicate the presence of additional transport mechanisms, which could be caused by density gradients or by the overlying wind field. As the match of the ratios varies dependent on the imposed wind condition, it is likely that wind influence varies between gas types. The impact of wind is discussed further in the following section.

4.2. Influence of Wind Condition

Wind influence on steady-state concentration distributions is small (Transport Case 1; see Figure 5a). However, we observe a tendency for concentrations to be lower under higher wind velocities. Deviations between sensor concentrations of different wind conditions can reach up to 7 percentage points. The depth to which concentration values are affected by a change in wind velocity varies dependent on the gas type. For CO_2 and N_2, only the upper half of the sand tank is affected, whereas for He, the effect is visible at all observed locations. Thus, affected locations correspond to the area where diffusive flux is likely to dominate over advective flux, indicating that an increase in wind velocity enhances diffusive fluxes inside the tank. This is likely to be caused by the effect of the wind velocity profile on the concentrations at the soil surface (see, e.g., observations made by Chamindu Deepagoda et al., 2018). With an increase of wind velocity, the thickness of the laminar boundary layer decreases, which reduces soil surface concentrations and increases concentration gradients between soil and atmosphere. Therefore, upward-directed diffusive fluxes depend on the wind velocity, which thereby also affects the concentration profiles inside the soil. An increase of mixing would also be expected due to the presence of turbulence-induced pressure pumping, which has been shown to be relevant for more permeable media than the one chosen here (e.g., Levintal et al., 2019; Poulsen, 2019). Following observations will confute its relevance to the present experiments.

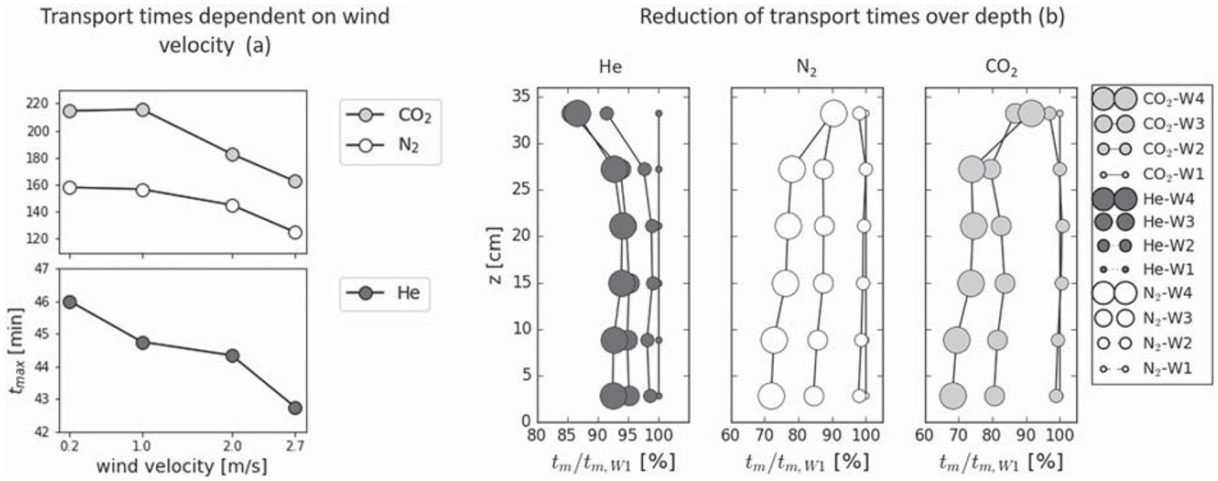

Figure 6. (a) Transport times measured at sensor OC6 (t_{max}) depending on wind velocity. Due to the high differences between He and the other two gases, He is displayed separately. (b) Depth-dependent reduction of transport times due to wind velocity shown by ratios of measured transport time t_m and transport times measured under the lowest wind velocity $t_{m,W1}$.

The influence of imposed wind condition is more apparent during the subsequent transient transport (Case 2). In line with previous studies, an increase in wind velocity fastens transport inside the sand tank and thereby exchange between soil and wind tunnel, despite relatively low soil permeabilities in comparison to those tested previously. This is valid for all three gas types, which is demonstrated in Figure 6a by displaying maximum measured transport times dependent on wind velocity. Transport times for He reduce linearly with wind velocity, whereas N_2 and CO_2 show stronger reductions between Wind Conditions W2, W3, and W4 than between W1 and W2. This gives further indication that sensitivity to the wind condition differs between gas types. Figure 6b shows that reduction of transport times by wind velocity is relatively constant over sand tank depth, except close to the soil surface. The profiles display the ratio between measured transport times (t_m) and the transport time measured under the lowest wind velocity ($t_{m,W1}$). We note that the ratios at Sensor Row 1 might be unreliable since concentration measurements are less accurate than at lower sensors due to overall low concentrations close to the surface and due to the shortness of transport times. Corresponding breakthrough curves show less differences between wind conditions than deeper sensors, which might be caused by the dominance of upward-directed diffusive flux over wind-induced transport. Diffusive fluxes close to the surface are especially high in the beginning of Transport Case 2 due to high concentration gradients. The shapes of the $t_m/t_{m,W1}$ profiles indicate that turbulence-induced pressure pumping did not play a pronounced role in the present study. Its presence is commonly understood to cause enhanced dispersive mixing, which is strongest close to the surface and decreases with depth. As was shown in Pourbakhtiar et al. (2017), this leads to very distinct profiles of transport times, where reduction due to an increase in wind velocity is strongest at the surface and decreases with porous medium depth. As here, reduction of t_m is more or less independent of depth, wind-induced dispersion is unlikely to be relevant to the conducted experiments. Note that for Figure 6b, t_m was defined as the time period between termination of gas supply until gas concentrations drop below 3 Vol-%. Although the differences between initial conditions among experiments conducted with the same gas type were only small, we eliminate all dependency on the initial condition by searching the highest common concentration span between experiments of same gas type to calculate t_m. Thus, $t_m/t_{m,W1}$ profiles serve for comparisons between experiments with different wind velocities, but not between different gas types.

We further note that our measurements suggest the presence of unintended transport effects around the gas inlet. Corresponding breakthrough curves show a rapid drop of concentration values directly after the termination of gas supply. The observed drop increases for higher wind velocities and is stronger on CO_2 and N_2 than on He (see Figure 5b Sensor Row 5 under Wind Condition W4 or Figures S3–S5 for all sensor breakthrough curves). Repeatability of the effect was confirmed by replicate experiments. Since its occurrence is limited to the vicinity of the gas inlet, we consider the existence of pressure fluctuations inflicted by the sudden termination of gas supply. Alternatively, transport around the gas inlet possibly accelerated due to the presence of preferential pathways. Even though the resulting effects are observable, they do not dominate over the influence of gas type or of wind condition but rather enhance the difference between tested conditions.

4.3. Wind-Induced Horizontal Transport

During steady-state gas supply (Transport Case 1), independent of the tested condition, concentration values at the wind-downstream side (transect OC) are higher than on the upstream side (transect OA). This is shown in Figure 7, which displays deviations Δc_{AC} between OA sensors and OC sensors of same height ($\Delta c_{AC} = c_{OA} - c_{OC}$). Although observed deviations are small (<3 Vol-%), their profiles follow specific patterns, which were confirmed by replicate experiments. We were able to eliminate a dependency on heterogeneous packing or nonuniform injection from the inlet by running a reference experiment without the influence of wind (the sand tank was closed up by a lid, and a gas outlet was placed at the lid's center. Δc_{AC} values were less than 0.3 Vol-% at all observed locations). For N_2 and CO_2, deviations between the left and the right occur mainly in the upper part of the sand tank. The relation between wind condition and strength of the asymmetry is unclear. Highest deviations occur under both the highest and lowest wind velocities (W1 and W4), but at different locations along z. For He, the asymmetrical effect is also strongest in the upper 15 cm of the tank, but it is not limited to this depth. Maximum deviations are located deeper than for the other two gases, and Δc_{AC} increases with wind velocity. There are two factors, which can cause the observed horizontal concentration gradients inside the tank. Although usually neglected, the near-surface

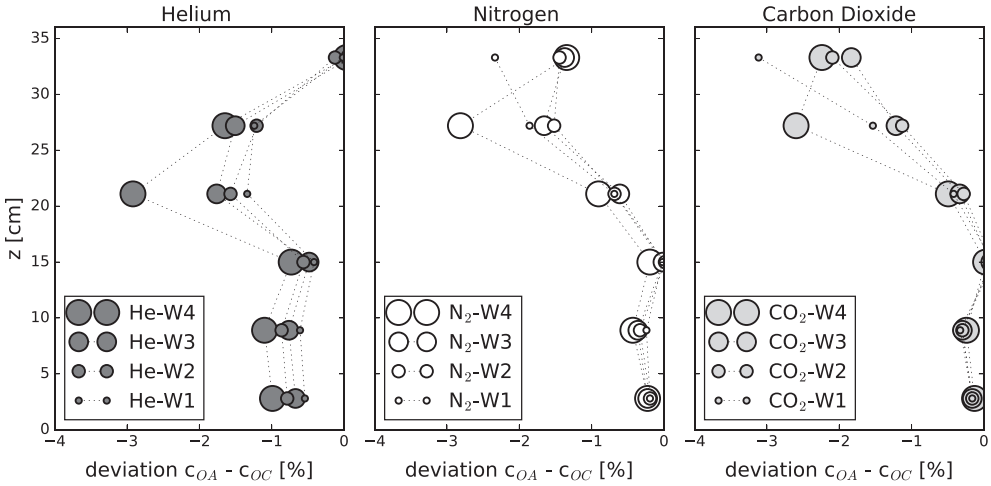

Figure 7. Profiles of deviations between sensor transects OA and OC. Marker size increases for increasing wind velocity.

wind field transfers momentum to the gas phase inside the pores of the soil. If the shear stresses are not balanced by friction or other counteracting forces (e.g., pressure or density gradients), wind creates advective transport in the subsurface, likely in wind direction, parallel to the soil surface (wind-induced horizontal advection). The effect is expected to increase with an increase in wind velocity. Second, gas component concentrations above the soil surface increase in wind-downstream direction due to the accumulation of gas components inside the laminar boundary layer (as has been shown by Chamindu Deepagoda, Smits, & Oldenburg, 2016; Chamindu Deepagoda et al., 2018). Consequently, concentration gradients across the surface are higher at the wind-upstream side of the sand tank than at the downstream side, thereby causing lower concentrations at transect OA than at transect OC. The relevance of this factor depends on the extent of the laminar boundary layer. Thus, it is expected to increase for decreasing wind velocities, in contrast to the prior factor. Considering the presence of both wind-induced advection and an unevenly distributed concentration layer, we can explain why strongest asymmetries occur for both the highest and lowest wind velocities in case of N_2 and CO_2 experiments. For He, one can assume that horizontal concentration gradients are caused by wind-induced advection rather than by the

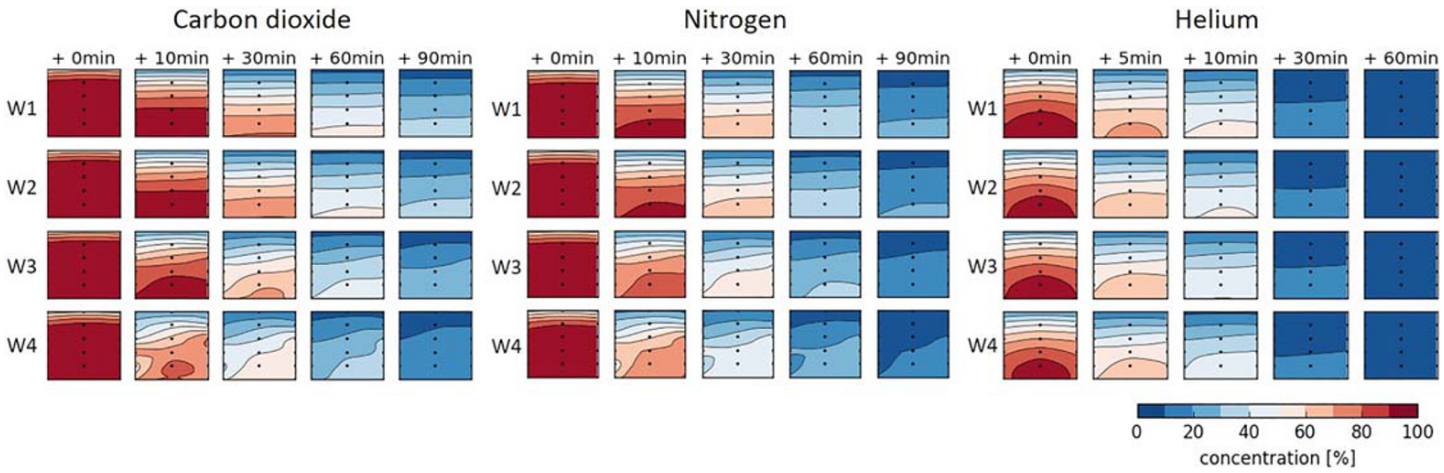

Figure 8. Interpolation of measured concentration values at steady-state gas supply (+0 min) and at 5, 10, 20, 30, and 60 min after termination of gas supply. Cubic interpolation between OA, OB, and OC sensors; black dots show the sensor placements. Note that concentrations are not extrapolated toward the sand tank boundaries.

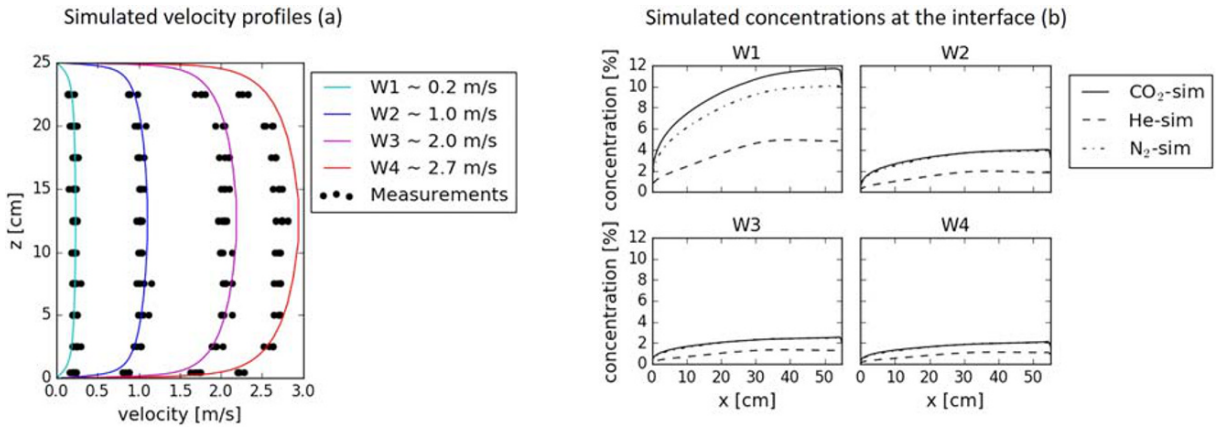

Figure 9. (a) Comparison of simulated and measured time-averaged velocity profiles inside the wind tunnel/free flow. Dots represent time-averaged measurements of wind velocity for all experiments. (b) Simulated concentration distributions directly above the interface at steady-state gas supply.

uneven concentration layer. This is only reasonable, since soil surface concentrations of He will be much smaller than those of N_2 and CO_2, due to its high diffusion coefficient and buoyancy.

With the termination of gas supply (start of Transport Case 2), horizontal concentration gradients between the left and right sides of the sand tank increase immediately. This is shown in Figure 8, which displays interpolated concentration fields at different points in time. All gases show an increase in horizontal concentration gradients with increasing wind velocity, which suggests the presence of wind-induced horizontal advection. Similar effects were observed by Poulsen et al. (2018), who investigated CO_2 transport through a high-permeable material with overlying wind field. Our results underline the importance of this mechanisms since we show that it can also be relevant in soils with lower permeability and for lower wind velocities than previously tested. We also find that the sensitivity to wind-induced advection depends on the gas type. For CO_2, it appears from Wind Conditions W2 and W3 that a certain threshold in wind velocity is overcome for the wind field to introduce clearly visible horizontal concentration gradients into the sand tank. In contrast, horizontal gradients of N_2 gradually increase from Wind Condition W1 over W2 and W3 to W4. For He, all four wind conditions introduce asymmetrical effects into the system, and the shapes of the concentration distributions do not separate between the different wind conditions as clearly as for the other two gases. Also, asymmetry appears weaker than for the heavier gases, which is expected due to its high diffusion coefficient. The higher resistance of CO_2 to be impacted by wind-induced advection is likely due to its high density, which creates downward directed density gradients that counteract wind-induced transport. We note that interpolated concentration fields give further indication for the presence of preferential pathways, since we observe relatively high local gradients at the sand tank bottom, specifically around sensor OB5. As stated above, resulting effects do not dominate over the influence of gas type or of wind condition.

5. Model Results

5.1. Model Parametrization and Comparison to Experimental Results

Prior to the gas transport simulations, we fitted the parabolic boundary condition for the wind velocity in order to match the measured velocity profiles above the soil surface, which is not parabolic due to turbulence. Compared to the parabolic profile at the boundary, the profile at the domain center is fuller and shows a lower peak. We found that applying a factor of 1.5 to the wind velocity to be achieved (measured wind velocity $\overline{v}(z_{wt} = 12.5\,\text{cm})$) leads to a value for the boundary velocity v_{max}, which gives a sufficient match between measured and simulated velocity profiles above the soil surface (see Figure 9a). The chosen factor does apply well for Wind Conditions W1, W2, and W3. Smaller discrepancies are observed for Wind Condition W4, which are accepted for simplicity only.

Subsequently, a first set of transport simulations was carried out by applying the sand properties collected in Table 1 ($\phi = 0.33$ and $k = 1e-11\text{m}^2$). Tortuosity and dispersion were neglected ($\tau = 1$ and $\alpha = 0$), as we do

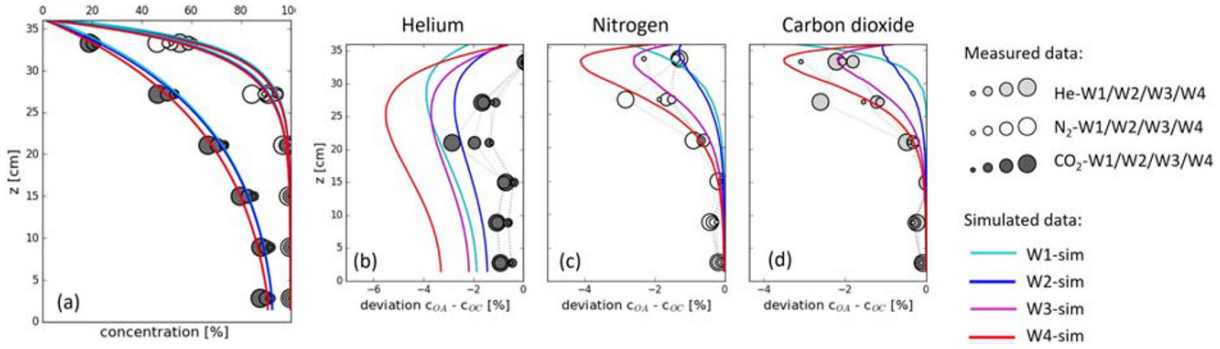

Figure 10. Comparison of simulated and measured concentrations under steady-state gas supply (Case 1) with fitted parameters ($\phi = 0.33$, $k = 2e-9\ m^2$, $\tau = 1$, and $\alpha = 0$). (a) Concentration profiles from horizontal averages of transects OA, OB, and OC. (b–d) Deviations between sensor transects OA and OC grouped by gas type.

not expect turbulence-induced dispersion to be relevant for the tested conditions. The model results were verified by comparison of measured and simulated gas concentrations inside the porous medium for both the steady-state and subsequent transient transport cases. The primary goal was to match the observed trends in regard to gas type and wind condition influence. It was not expected to achieve a perfect match to the experimental results, since some of the complexity of the experiments was neglected in the model (variations in atmospheric conditions, possible heterogeneity of the porous medium, and pressure fluctuations at the gas inlet). Although we do not have measurement data to verify the simulated concentrations inside the free flow, we can state that the predicted concentration layers at the soil surface are in agreement with observations made in Chamindu Deepagoda, Smits, and Oldenburg (2016) and Chamindu Deepagoda et al. (2018). As expected, surface concentrations increase along the surface in wind direction (see Figure 9b). Concentration values reduce for higher wind velocities and differ between gas types.

For the simulated concentration fields inside the porous medium, it was found that while overall match between measured and predicted concentrations is already high for Wind Condition W1, the model shows little sensitivity to an increase in wind velocity. Thus, match for higher wind conditions is comparably weak. An analysis of simulated streamlines showed that the transfer of momentum at the interface is too small to create any influence of wind on flow patterns inside the porous medium. Thus, wind impact is limited to the change of soil surface gas concentrations (as was shown in Figure 9b). Although this influences vertical

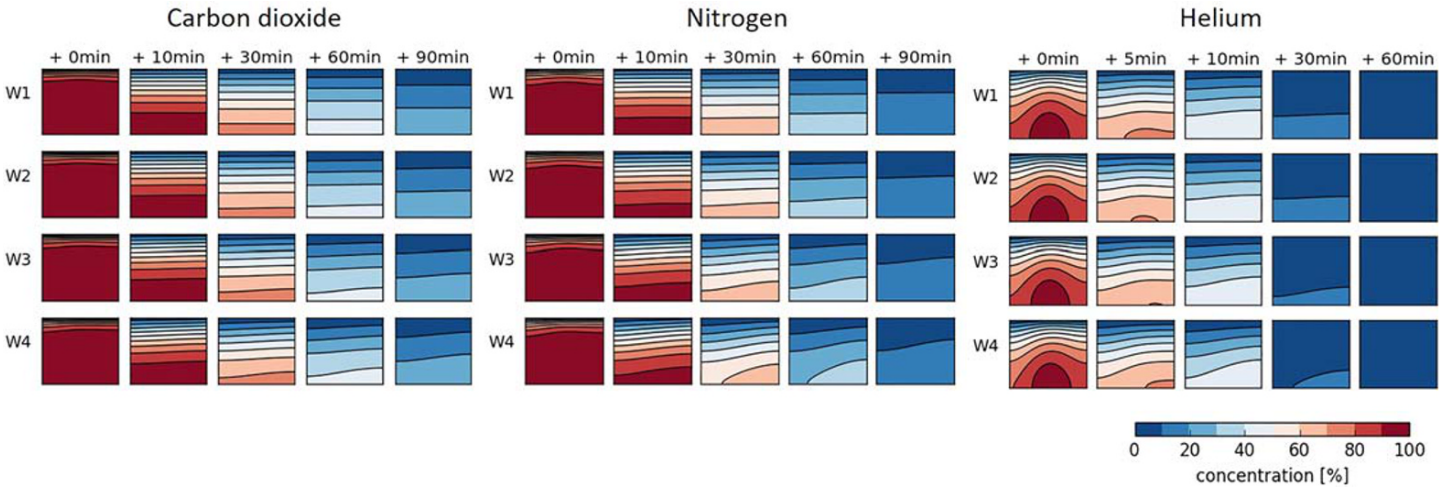

Figure 11. Simulated concentration fields at steady-state gas supply and at multiple time steps after termination of gas supply. Refer to Figure S7 for more time steps.

concentration gradients, resulting horizontal concentration gradients in the subsurface are negligible, indicating that observed concentration distributions showing high horizontal gradients must have been exposed to additional transport mechanisms such as wind-induced advection. We refer to Figures S6 and S7 for more information on the corresponding model results.

Subsequently, the model parameters were fitted. Each model parameter was varied separately to test the impact on model results. We found that sufficient asymmetry in the steady-state and in the transient concentration distributions can only be achieved by increasing the permeability of the porous medium. The porosity and the tortuosity coefficient impact the effective diffusivity but do not influence advective fluxes. Changing their values leads to uniform decreases or increases of transport times throughout the porous medium but does not produce any horizontal concentration gradients. We find that the overall transport behavior is well represented for all gas types and all wind conditions by increasing the permeability of the porous medium by 2 orders of magnitude ($k = 2e\text{-}9\ m^2$). Molecular diffusion coefficients are sufficient to meet overall transport times for all three gases. Thus, effective diffusion coefficients need no fitting by changing the tortuosity coefficient or by adding additional dispersion. This is indicated by well-matched model results under low wind forcing (see Wind Condition W1 in Figures S5 and S6). The final results of the parameter fitting are summarized in Figures 10 and 11. For Transport Case 1, concentration profiles are well matched, and an increase in wind velocity leads to a reduction of concentrations in the right order of magnitude (see Figure 10a). Also, the model is able to reproduce key characteristics of measured deviations between sensor transects OA and OC (see Figures 10b–10d). Although deviations for He are slightly overestimated, overall, deviations are in the right order of magnitude. Depth dependency is captured especially well for all three gas types. The model reproduces the characteristic drop toward the bottom and the top of the porous medium, which occurs for all tested conditions with the exception of CO_2 and N_2 under Wind Condition W1. For these two cases, deviations steadily increase toward the soil surface, which is also reproduced by the model. This is a strong indication that the model captures the relevant transport mechanisms and the coupling between porous medium and free flow, which can also be shown for Transport Case 2. Simulated concentration distributions for different points in time are given in Figure 11. Refer to Figure 8 for equivalent experimental results. The model qualitatively reproduces the strong asymmetrical distributions that occurred during Transport Case 2. Overall relations between gas types and wind influence are well represented: He is already affected by the smallest wind velocity, CO_2 is not affected by the low wind velocities (W1 and W2) but reacts to higher ones (W3 and W4), and for N_2, horizontal concentration gradients increase steadily with increasing wind velocities. The model does not reproduce the drop of concentrations around the gas inlet after the termination of gas supply or the local concentration gradients at the sand tank bottom, which were observed for N_2 and CO_2 under Wind Conditions W3 and W4. Thus, the simulated horizontal concentration gradients for these cases are not as strong as in the experiments. The patterns deviate especially at the beginning (e.g., at +10 min). This is further indication that transport at the tank bottom was influenced by heterogeneous packing or other factors not represented in the model.

Further indication of the absence of turbulence-induced pressure pumping is given by the reasonable well match between predicted and observed transport times without enhancing the effective diffusion coefficient inside the porous medium for higher wind velocities. The absence of pressure pumping due to wind turbulence could be due to the chosen sand and its comparable low permeability or due to the choice of wind velocities. Wind velocities are comparably low in comparison to other studies where wind-induced pressure pumping appeared to be relevant. The increase of permeability of 2 orders of magnitude compared to previously measured values for the sand is not expected to be realistic. The permeability is interpreted as an apparent parameter that allows to produce similar subsurface flow velocities to the ones that must have been occurred during experiments. With the original permeability, the model underestimates flow velocities either because the chosen coupling conditions underestimate the transfer of momentum at the interface or because flow inside the sand tank partly occurred along preferential pathways, which are not represented in the model. The existence of such flow paths is indicated by the measurements (see Transport Case 2). Different plausible preferential flow paths in the tank could be expected: flow along loose parts around the sensors (despite efforts to avoid such zones) or flow along the tank boundaries. As the experiments allow not for a determination of the paths, we do not attempt to reproduce exact flow patterns. The simulations show, however, that it is crucial to capture the coupling of flow between surface and subsurface to produce the observed transport behavior.

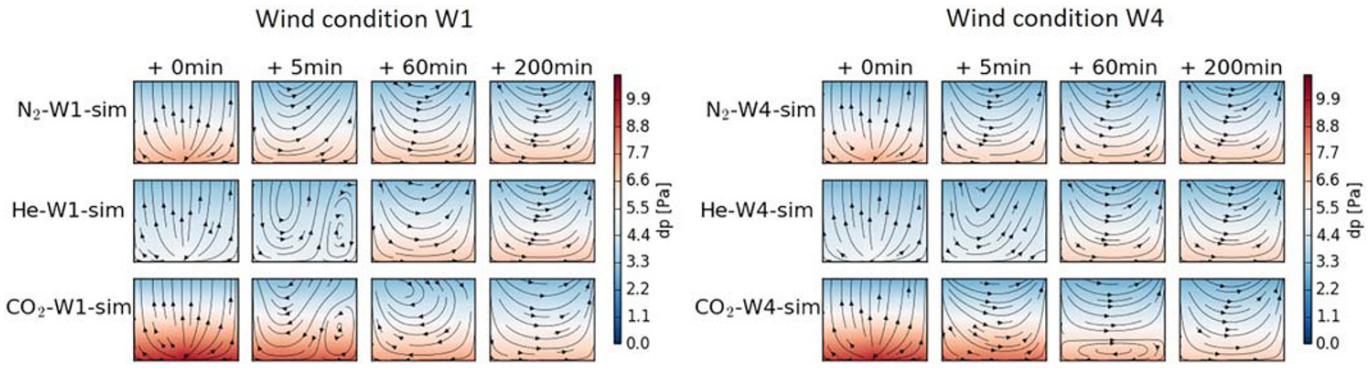

Figure 12. Simulated pressure fields and streamlines at certain points in time after termination of gas supply, exemplarily for Wind Conditions W1 and W4. Additional wind conditions and more time steps can be found in Figure S9.

5.2. Transport Mechanisms Controlling the Mass Exchange Between the Domains

The model results were analyzed to gain a deeper understanding of the relevant transport mechanisms that occur during wind exposure and to determine why wind effect on transport differs dependent on the characteristics of the transported component. To do so, we investigated simulated flow fields inside the porous medium and the composition of fluxes at the interface. Additionally, we tested the relevance of gas density by repeating all simulations without gravitation. The results are discussed below.

5.2.1. Transport Mechanisms Inside the Porous Medium

During steady-state gas supply (Transport Case 1), advective fluxes radiating from the gas source dominate over wind-induced advection. Streamlines point upwards since flow is channeled by the domain boundaries (see Figure 12 at +0 min). After the gas supply is stopped (Transport Case 2), pressure fields inside the porous medium rearrange (see Figures 12 and S9 for pressure fields for all wind conditions). The pressure field shows a clear dependency on the density distribution. Thus, for gases with a differing density to air (CO_2 and He), the pressure field depends on the concentration distribution of the particular gas. This dependency causes very unique flow patterns, which change over time and are highly dependent on the imposed wind condition. With decreasing gas concentrations inside the porous medium, streamlines eventually reach a new steady-state, where flow occurs along U-shaped lines in alignment to the tank walls. This is valid for all tested wind conditions and shows that the choice of domain boundaries is largely responsible for the direction of flow and the formation of flow patterns. A cross-checking of concentration levels and flow patterns shows that concentrations of He have to drop below 10 Vol-%, so no impact of density on flow patterns is visible. For the heavy gas CO_2, concentrations have to drop below 5 Vol-%. These concentration levels correspond to low wind velocities (W1). With an increase in wind velocity, critical concentration levels become higher and the steady-state U-shaped flow patterns are reached faster. When gravity is turned off from the

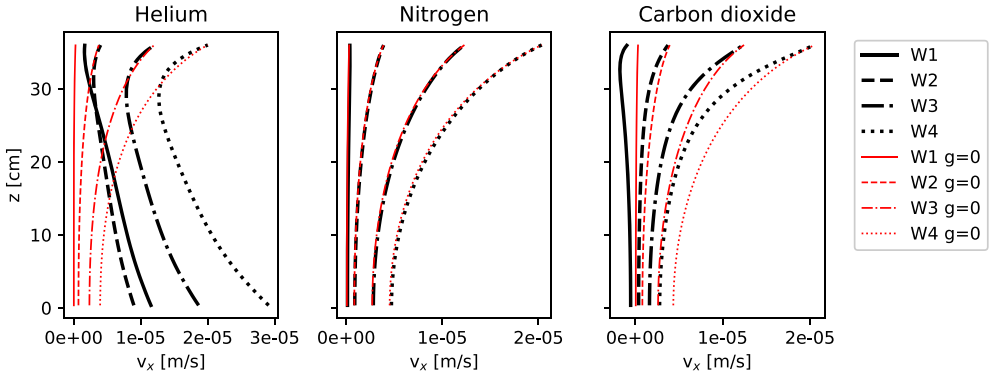

Figure 13. Vertical profiles of horizontal velocity (v_x) during steady-state gas supply. The profiles are obtained by horizontal averaging of simulated velocity fields. Red lines represent simulations without gravity ($g = 0$).

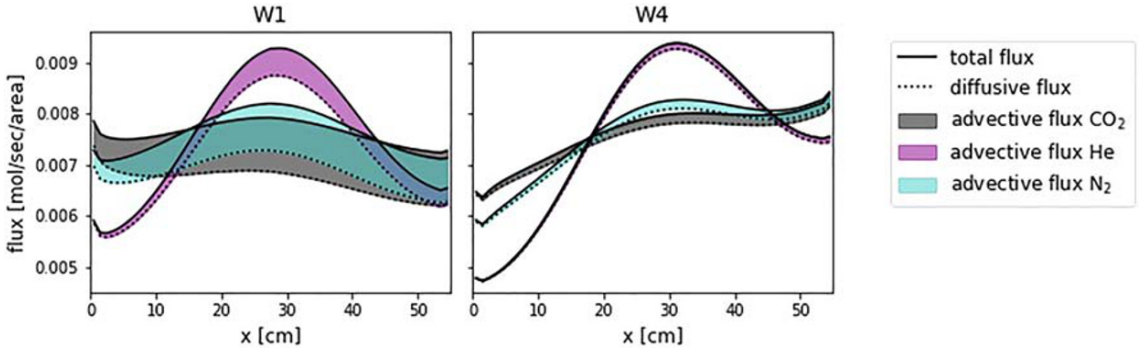

Figure 14. Flux composition at the interface for Transport Case 1, exemplarily for Wind Conditions W1 and W4.

model, flow fields are no longer density dependent to the effect that streamlines are U-shaped and time invariant over Transport Case 2 (see Figure S10).

The impact of imposed wind condition becomes apparent by comparing horizontal flow velocities along the depth of the porous medium. Figure 13 depicts vertical profiles of net horizontal velocity (v_x) during steady-state gas supply. Refer to the black lines for simulation results with gravity.

The profiles show that horizontal advective flux increases for higher wind velocities. v_x points in wind-downstream direction and increases with wind velocity. Similar effects are observed for the transient transport case (see exemplarily v_x at 30 min after termination of gas supply in Figure S11). Although v_x values lie in the same order of magnitude for all three gases, the penetration depth of momentum depends on the gas type. For the heavy and density-neutral gases (CO_2 and N_2), v_x is highest at the surface and reduces toward the bottom. The opposite holds for He. Without gravity (red lines), horizontal velocities are purely wind induced to the effect that v_x values decrease with depth and show no apparent difference between gas types. This observation indicates that the sensitivity to wind-induced advection does not depend on the viscosity or the diffusion coefficient of the transported components but on its density. For CO_2, v_x values increase in comparison to the results with gravity, showing that its high density lessens its sensitivity to wind-induced advection. For He, its low density triggers a high sensitivity to wind-induced advection. The changes in the flow field due to gravity do affect the concentration distribution inside the porous medium. A comparison of simulated concentration fields shows that density is largely responsible for the difference in horizontal concentration gradients between gas types.

5.2.2. Transport Mechanisms at the Interface

The presence of wind-induced horizontal flows ultimately changes the distribution of soil gas emissions from the surface. In Figure 14, flux distributions are shown for steady-state gas supply (Transport Case 1). Under low wind forcing (Wind Condition W1), the distribution of flux at the surface reflects the placement of the gas source: Flux is strongest at the center of the interface and drops to both sides. The peak of flux at the center of the interface is stronger the lighter the gas. The difference of flux distributions between gas types is due to buoyancy, which was confirmed by comparing the results of simulations with and without

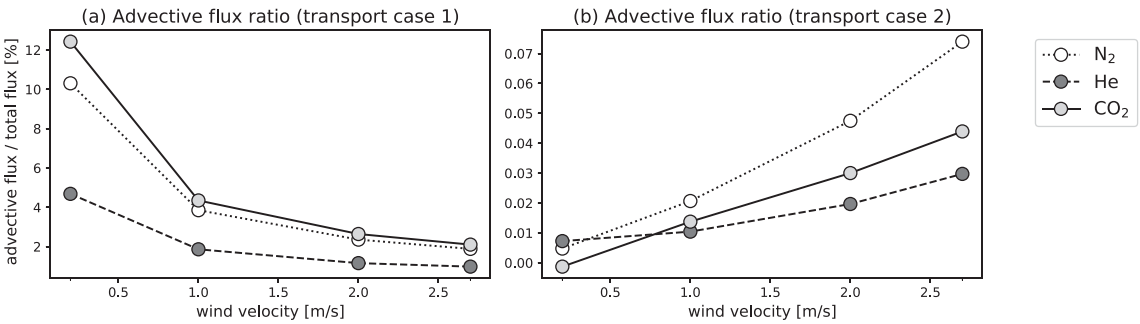

Figure 15. Advective flux ratios across the interface dependent on wind velocity during steady-state gas supply (a) and 30 min after termination of gas supply (b).

gravity (see Figure S12). A raise in wind velocity leads to an increase of flux along the surface in wind direction. This effect is stronger the lighter the gas. Similar effects are observed during the transient transport case (see Figure S13). The total flux across the interface decomposes into a diffusive and an advective part. Despite the presence of the gas source, the dominating driver for the soil gas emissions is diffusion. Advection makes out 1% to 12% of total flux across the interface during steady-state gas supply. It decreases with wind velocity (see Figures 14 and 15a), because a raise in wind velocity decreases soil surface concentrations and thereby increases vertical concentration gradients at the interface. Thus, an increase in wind velocity enhances diffusive fluxes from the soil surface to the effect that advective ratios decrease.

With the start of Transport Case 2, the gas source no longer drives the system to the effect that advection at the interface immediately drops to less than 0.2% of total flux. The remaining advective transport across the interface is purely wind induced. This is indicated by Figure 15b, which shows that advective ratios of total flux raise with increasing wind velocity. We conclude that for the tested conditions, wind-induced advection shows only minor contributions to the overall gas exchange between soil and atmosphere. However, it indirectly affects the diffusive fluxes across the interface due to horizontal transport in the subsurface, which changes the concentration distribution and thereby the concentration gradients, which drive diffusion. Wind-induced advection is also responsible for changing the position of gas discharge at the soil surface. Its contribution to soil-atmosphere gas exchange is likely to increase for higher wind velocities or higher soil permeabilities.

6. Summary and Discussion

Experimental and numerical results demonstrate that flow and transport in the vicinity of the soil surface is strongly coupled to the overlying near-surface wind field. The presence of transported components with pronounced density difference to air adds additional complexity to the transport through the wind-affected soil layers. The resulting transport is clearly multidimensional. Relevant transport mechanisms are molecular diffusion and advection with flow fields caused by pressure and density gradients as well as wind-induced advection.

The results indicate that for the tested soil and the tested wind conditions, soil-atmosphere gas exchange is not affected by turbulence-induced pressure pumping. This is in line with previous studies that show a decreasing relevance of this factor for lower permeable porous media (Acharya & Prihar, 1969; Levintal et al., 2019). However, experimental results show that an increase in wind velocity can still lead to an acceleration of mass exchange at the interface and to substantial changes in subsurface transport. The numerical investigation demonstrates that this is due to the reduction of soil surface gas concentration that increases vertical concentration gradients and thereby upward-directed diffusion and also due to wind-induced subsurface advection. Wind-induced advection is caused by transfer of momentum from the wind field into the soil. Although the ratio of mass flux caused by advection is much smaller than mass flux caused by diffusion, wind-induced advection can lead to explicit changes in the subsurface concentration distribution and thus changes diffusive mass fluxes. This is observed for both tested transport cases: transport driven by a buried point source with constant gas supply and subsequent transient transport under decreasing concentration gradients. In both cases wind-induced advection leads to subsurface horizontal gas transport with wind direction. As shown by the model results, this ultimately changes the location of soil gas discharge at the surface. The numerical investigation reveals that domain boundaries are largely responsible for the direction of flow and the formation of flow patterns inside the porous medium. This goes to show that experimental findings cannot be readily transferred to the field. Assumptions made based on experimental data, where flow in a porous medium is confined by boundaries, have to be taken into question, and the sensitivity of results to the chosen domain boundaries should be further investigated. However, wind-induced horizontal advection can be expected to become even more relevant, when flow is not bounded in horizontal direction. Previous studies demonstrate the relevancy of wind-induced advection in highly permeable porous media (Poulsen, Furman, & Liberzon, 2017; Poulsen et al., 2018; Poulsen, 2018, 2019): gravels and marble rock as well as very coarse sand with air permeabilities $>1e-9\ m^2$). Our results expand the field of porous media for which wind-induced advection can be a relevant transport mechanisms, as we show the existence of it in a low permeable fine sand (estimated air permeability of $1e-11\ m^2$). Further investigations should be considered

to test its occurrence at larger scales, in real soils, and under natural wind conditions, when the main wind direction is not as pronounced as in the laboratory.

Density gradients caused by the presence of gases with a strong density difference to air influence the transport processes inside the wind-exposed soil layers. Consequently, wind effects differ dependent on the characteristics of the transported component itself. Exemplarily, we observe that wind-induced advection affects transport of light gases already at low wind velocity, whereas it appears that for heavier gases, a certain threshold in wind velocity has to be reached for wind influence to become visible. The results also indicate that the depth of impact of wind increases for transport of light gases. The model results reveal that flow patterns strongly depend on the combination of wind forcing at the atmospheric boundary and the density distribution inside the porous medium. It is clearly visible that density gradients cause complex multidimensional transport processes for all tested wind conditions and that light as well as heavy gases cannot be treated as inert tracers. Model results also show that the density of the transported component determines the sensitivity to wind-induced (horizontal) advection. We note that results also indicate that density effects on the flow exist only for sufficiently high concentration levels. Thus, density effects will mostly be expected for transport problems where high gas concentrations are likely to occur. This is valid for gas releases from subsurface anthropogenic sources and less likely for natural gas production by biological processes. Given the fact that CO_2 is the most used tracer gas in laboratory assessments of soil-atmosphere gas exchange, we recommend to use N_2 as a tracer instead of CO_2, if density effects are to be avoided.

Our findings generally indicate that gas transport in the vicinity of the soil surface is multidimensional and horizontal fluxes can be of relevant order of magnitude. Thus, the applicability of standard one-dimensional modeling approaches, which only consider vertical gas movement for approximating soil gas emissions, must be taken under consideration. We demonstrate that the relevant transport mechanisms can be captured with coupled porous medium-free flow models. The results indicate the importance of representing the wind field by turbulence models, since soil surface gas concentration shows to be strongly dependent on the near-surface wind velocities and turbulent mixing coefficients. Model results show a reasonable well match to the experimental data without extensive fitting of model parameters. The only parameter, which had to be fitted, is the air permeability of the porous medium, as the model did not produce wind-induced subsurface advection in the right order of magnitude. The air permeability had to be increased by 2 orders of magnitude. Increasing this parameter to such extent compensates for factors that are not well represented or neglected in the model. We consider it probable that flow inside the porous medium was partly influenced by the unintended presence of preferential pathways along sensors or along the walls of the porous medium. Preferential pathways lead to local increases of air permeability, which are not represented in the model. The existence of preferential flow is even more likely to occur in real soils. Thus, if preferential flow paths were responsible for amplifying the differences of results between tested conditions, this is also likely to occur under natural conditions in the field. Another reason why the model underestimates wind-induced advection for the original air permeability might be the chosen coupling conditions at the interface, specifically the coupling of momentum. As the particular coupling condition depends on the permeability of the porous medium, an underestimation of momentum exchange by the design of the condition can be compensated by increasing the air permeability. The chosen conditions clearly simplify the properties of that interface, since they assume it to be sharp and smooth. Including coupling concepts that consider surface roughness as presented by Fetzer et al. (2016) could increase the performance of the model and should be tested in future studies. Overall, we demonstrate the need of coupled multidimensional numerical models such as presented to capture the interactions between subsurface gas transport and the overlying wind field correctly and to accurately predict exchange rates between the soil and the atmosphere. Such models will most likely not replace one-dimensional modeling approaches for larger-scale applications, because of the comparably high computational effort. Notwithstanding, they can help us gain a deeper understanding of the relevant processes and to determine the limitations of the applicability of one-dimensional modeling approaches.

Data Availability Statement

Experimental data and model codes are currently being archived in the Zenodo repository (experimental data: 10.5281/zenodo.3736191; model code: 10.5281/zenodo.3902190).

Acknowledgments
This work has been funded by the German Research Foundation (Deutsche Forschungsgemeinschaft [DFG]) under Projects NE 824/14-1 and 327154368 and by the U.S. National Science Foundation under Project 1447533. We thank the DFG and the U.S. National Science Foundation for their support.

References

Acharya, C. L., & Prihar, S. S. (1969). Vapor losses through soil mulch at different wind velocities[1]. *Agronomy Journal*, *61*(5), 666–668. https://doi.org/10.2134/agronj1969.00021962006100050004x

Altevogt, A. S., Rolston, D. E., & Venterea, R. T. (2003). Density and pressure effects on the transport of gas phase chemicals in unsaturated porous media. *Water Resources Research*, *39*(3), 1061. https://doi.org/10.1029/2002WR001338

Basirat, F., Sharma, P., Fagerlund, F., & Niemi, A. (2015). Experimental and modeling investigation of CO_2 flow and transport in a coupled domain of porous media and free flow. *International Journal of Greenhouse Gas Control*, *42*, 461–470. https://doi.org/10.1016/j.ijggc.2015.08.024

Bear, J. (1961). On the tensor form of dispersion in porous media. *Journal of Geophysical Research*, *66*(4), 1185–1197. https://doi.org/10.1029/jz066i004p01185

Beavers, G. S., & Joseph, D. D. (1967). Boundary conditions at a naturally permeable wall. *Journal of Fluid Mechanics*, *30*(1), 197–207. https://doi.org/10.1017/S0022112067001375

Bowling, D. R., & Massman, W. J. (2011). Persistent wind-induced enhancement of diffusive CO_2 transport in a mountain forest snowpack. *Journal of Geophysical Research*, *116*, G04006. https://doi.org/10.1029/2011JG001722

Chamindu Deepagoda, T. K. K., Mitton, M., & Smits, K. (2018). Effect of varying atmospheric conditions on methane boundary-layer development in a free flow domain interfaced with a porous media domain. *Greenhouse Gases: Science and Technology*, *8*(2), 335–348. https://doi.org/10.1002/ghg.1743

Chamindu Deepagoda, T. K. K., Smits, K. M., & Oldenburg, C. M. (2016). Effect of subsurface soil moisture variability and atmospheric conditions on methane gas migration in shallow subsurface. *International Journal of Greenhouse Gas Control*, *55*, 105–117. https://doi.org/10.1016/j.ijggc.2016.10.016

Chamindu Deepagoda, T. K. K., Smits, K., Ramirez, J., & Moldrup, P. (2016). Characterization of thermal, hydraulic, and gas diffusion properties in variably saturated sand grades. *Vadose Zone Journal*, *15*(4), vzj2015.07.0097. https://doi.org/10.2136/vzj2015.07.0097

Davarzani, H., Smits, K., Tolene, R. M., & Illangasekare, T. (2014). Study of the effect of wind speed on evaporation from soil through integrated modeling of the atmospheric boundary layer and shallow subsurface. *Water Resources Research*, *50*, 661–680. https://doi.org/10.1002/2013WR013952

Falta, R. W., Javandel, I., Pruess, K., & Witherspoon, P. A. (1989). Density driven flow of gas in the unsaturated zone due to the evaporation of volatile organic compounds. *Water Resources Research*, *25*(10), 2159–2169. https://doi.org/10.1029/WR025i010p02159

Fetzer, T., Smits, K. M., & Helmig, R. (2016). Effect of turbulence and roughness on coupled porous-medium/free-flow exchange processes. *Transport in Porous Media*, *114*(2), 395–424. https://doi.org/10.1007/s11242-016-0654-6

Gao, B., Davarzani, H., Helmig, R., & Smits, K. M. (2018). Experimental and numerical study of evaporation from wavy surfaces by coupling free flow and porous media flow. *Water Resources Research*, *54*, 9096–9117. https://doi.org/10.1029/2018WR023423

Glass, R. J., Conrad, S. H., & Peplinski, W. (2000). Gravity-destabilized nonwetting phase invasion in macroheterogeneous porous media: Experimental observations of invasion dynamics and scale analysis. *Water Resources Research*, *36*(11), 3121–3137. https://doi.org/10.1029/2000WR900152

Haghighi, E., & Or, D. (2015). Evaporation from wavy porous surfaces into turbulent airflows. *Transport in Porous Media*, *110*(2), 225–250. https://doi.org/10.1007/s11242-015-0512-y

Hanks, R. J., & Woodruff, N. P. (1958). Influence of wind on water vapor transfer through soil, gravel, and straw mulches. *Soil Science*, *86*(3), 160–164. https://doi.org/10.1097/00010694-195809000-00010

Helmig, R. (1997). Multiphase flow and transport processes in the subsurface: A contribution to the modeling of hydrosystems.

Ishihara, Y., Shimojima, E., & Harada, H. (1992). Water vapor transfer beneath bare soil where evaporation is influenced by a turbulent surface wind. *Journal of Hydrology*, *131*(1-4), 63–104. https://doi.org/10.1016/0022-1694(92)90213-F

Jang, W., & Aral, M. M. (2007). Density-driven transport of volatile organic compounds and its impact on contaminated groundwater plume evolution. *Transport in Porous Media*, *67*(3), 353–374. https://doi.org/10.1007/s11242-006-9029-8

Koch, T., Gläser, D., Weishaupt, K., Ackermann, S., Beck, M., Becker, B., et al. (2020). $DuMu^x$ 3—An open-source simulator for solving flow and transport problems in porous media with a focus on model coupling. *Computers and Mathematics with Applications*. https://doi.org/10.1016/j.camwa.2020.02.012

Laemmel, T., Mohr, M., Schack-Kirchner, H., Schindler, D., & Maier, M. (2017). Direct observation of wind-induced pressure-pumping on gas transport in soil. *Soil Science Society of America Journal*, *81*(4), 770–774. https://doi.org/10.2136/sssaj2017.01.0034n

Levintal, E., Dragila, M. I., & Weisbrod, N. (2019). Impact of wind speed and soil permeability on aeration time in the upper vadose zone. *Agricultural and Forest Meteorology*, *269-270*, 294–304. https://doi.org/10.1016/j.agrformet.2019.02.009

Lou, X. F., & Nair, J. (2009). The impact of landfilling and composting on greenhouse gas emissions—A review. *Bioresource Technology*, *100*(16), 3792–3798. https://doi.org/10.1016/j.biortech.2008.12.006

Maier, M., Schack-Kirchner, H., Aubinet, M., Goffin, S., Longdoz, B., & Parent, F. (2012). Turbulence effect on gas transport in three contrasting forest soils. *Soil Science Society of America Journal*, *76*(5), 1518–1528. https://doi.org/10.2136/sssaj2011.0376

Maier, M., Schack-Kirchner, H., Hildebrand, E. E., & Holst, J. (2010). Pore-space CO_2 dynamics in a deep, well-aerated soil. *European Journal of Soil Science*, *61*(6), 877–887. https://doi.org/10.1111/j.1365-2389.2010.01287.x

Massman, W. J., Sommerfeld, R. A., Mosier, A. R., Zeller, K. F., Hehn, T. J., & Rochelle, S. G. (1997). A model investigation of turbulence-driven pressure-pumping effects on the rate of diffusion of CO_2, N_2O, and CH_4 through layered snowpacks. *Journal of Geophysical Research*, *102*(15), 18,851–18,863. https://doi.org/10.1029/97jd00844

Mohr, M., Laemmel, T., Maier, M., & Schindler, D. (2016). Analysis of air pressure fluctuations and topsoil gas concentrations within a Scots pine forest. *Atmosphere*, *7*(10), 125. https://doi.org/10.3390/atmos7100125

Mosthaf, K., Helmig, R., & Or, D. (2014). Modeling and analysis of evaporation processes from porous media on the REV scale. *Water Resources Research*, *50*, 1059–1079. https://doi.org/10.1002/2013WR014442

Oertel, C., Matschullat, J., Zurba, K., Zimmermann, F., & Erasmi, S. (2016). Greenhouse gas emissions from soils: A review. https://doi.org/10.1016/j.chemer.2016.04.002

Poulsen, T. G. (2018). Measuring horizontal pore gas velocity profiles in porous media in response to near-surface wind speed and gustiness. *European Journal of Soil Science*, *69*(6), 997–1007. https://doi.org/10.1111/ejss.12722

Poulsen, T. G. (2019). Linking below-surface horizontal pore velocity profiles in porous media with near-surface wind conditions and porous medium gas permeability. https://doi.org/10.1111/ejss.12833

Poulsen, T. G., Furman, A., & Liberzon, D. (2017). Effects of wind speed and wind gustiness on subsurface gas transport. *Vadose Zone Journal*, *16*(11), vzj2017.04.0079. https://doi.org/10.2136/vzj2017.04.0079

Poulsen, T. G., Furman, A., & Liberzon, D. (2018). Effect of near-surface wind speed and gustiness on horizontal and vertical porous medium gas transport and gas exchange with the atmosphere. *European Journal of Soil Science*, *69*(2), 279–289. https://doi.org/10.1111/ejss.12531

Poulsen, T. G., & Møldrup, P. (2006). Evaluating effects of wind-induced pressure fluctuations on soil-atmosphere gas exchange at a landfill using stochastic modelling. *Waste Management & Research: The Journal of the International Solid Wastes and Public Cleansing Association, ISWA*, *24*(5), 473–81. https://doi.org/10.1177/0734242X06066363

Poulsen, T. G., Pourber, A., Furman, A., & Papadikis, K. (2017). Relating wind-induced gas exchange to near-surface wind speed characteristics in porous media. *Vadose Zone Journal*, *16*(8), vzj2017.02.0039. https://doi.org/10.2136/vzj2017.02.0039

Poulsen, T. G., & Sharma, P. (2011). Apparent porous media gas dispersion in response to rapid pressure fluctuations. *Soil Science*, *176*(12), 635–641. https://doi.org/10.1097/SS.0b013e3182372fae

Pourbakhtiar, A., Poulsen, T. G., Wilkinson, S., & Bridge, J. W. (2017). Effect of wind turbulence on gas transport in porous media: Experimental method and preliminary results. *European Journal of Soil Science*, *68*(1), 48–56. https://doi.org/10.1111/ejss.12403

Reid, R. C., Sherwood, T. K., & Street, R. E. (1959). The properties of gases and liquids. *Physics Today*, *12*(4), 38–40. https://doi.org/10.1063/1.3060771

Saffman, P. G. (1971). On the boundary condition at the surface of a porous medium. *Studies in Applied Mathematics*, *50*(2), 93–101. https://doi.org/10.1002/sapm197150293

Scanlon, B. R., Nicot, J. P., & Massmann, J. W. (2001). Soil gas movement in unsaturated systems. *Soil physics companion* (pp. 297–341). Boca Raton, FL: CRC Press. https://doi.org/10.1201/9781420041651.ch8

Scheidegger, A. E. (1961). General theory of dispersion in porous media. *Journal of Geophysical Research*, *66*(10), 3273–3278. https://doi.org/10.1029/jz066i010p03273

Sleep, B. E. (1998). Modeling transient organic vapor transport in porous media with the dusty gas model. *Advances in Water Resources*, *22*(3), 247–256. https://doi.org/10.1016/S0309-1708(98)00011-6

Smits, K. M., Sakaki, T., Limsuwat, A., & Illangasekare, T. H. (2010). Thermal conductivity of sands under varying moisture and porosity in drainage wetting cycles. *Vadose Zone Journal*, *9*(1), 172. https://doi.org/10.2136/vzj2009.0095

Ulrich, B. A., Mitton, M., Lachenmeyer, E., Hecobian, A., Zimmerle, D., & Smits, K. M. (2019). Natural gas emissions from underground pipelines and implications for leak detection. *Environmental Science and Technology Letters*, *6*(7), 401–406. https://doi.org/10.1021/acs.estlett.9b00291

Van Driest, E. R. (1956). On turbulent flow near a wall. *Journal of the Aeronautical Sciences*, *23*(11), 1007–1011. https://doi.org/10.2514/8.3713

Wilcox, D. C. (1993). *Turbulence modeling for CFD* (Vol. 93). La Canada, CA: DCW Industries.